Journal of Hazardous Materials 395 (2020) 122666

Contents lists available at ScienceDirect

Journal of Hazardous Materials

journal homepage: www.elsevier.com/locate/jhazmat

Nano-Fe mediated treatment of real hydraulic fracturing flowback and its practical implication on membrane fouling in tandem anaerobic-oxic membrane bioreactor

Olusegun K. Abass[a,b,c,*], Kaisong Zhang[a,*]

[a] CAS Key Laboratory of Urban Pollutant Conversion, Institute of Urban Environment, Xiamen 361021, China
[b] University of Chinese Academy of Sciences, Beijing 100049, China
[c] School of Civil and Environmental Engineering, Nanyang Technological University, 639798, Singapore

GRAPHICAL ABSTRACT

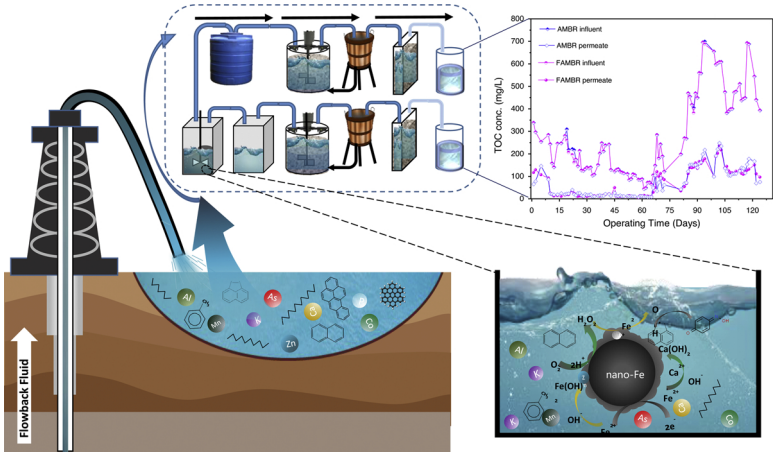

ARTICLE INFO

Editor: Daniel C.W. Tsang.

Keywords:
Hydraulic fracturing flowback
Membrane bioreactor
Membrane fouling
Fe nanomaterials
PAHs

ABSTRACT

The rising water-use intensity, and lack of cost-effective treatment strategy and reuse of hydraulic fracturing flowback (HFF) has become an increasing cause of concern. The present work evaluates the integration of parallel sets of tandem anaerobic-oxic membrane bioreactor (AMBR) with and without nano-Fe for treatment and reuse of real HFF obtained from Ordos Basin, China. Treatment efficiencies in terms of organic conversions, micro-pollutants degradation, resource recovery, and effects of nano-Fe release on membrane fouling were evaluated. Nano-Fe mediated AMBR (FAMBR) system effectively reduce target micro-pollutants (such as Acenaphthylene) at 94.4 % compared to the parallel AMBR system (17.1 % without nano-Fe). Moreover, recovery of potential economic chemicals like Al and P (1.0 and 0.6 mg/g spent nano-Fe) availed using FAMBR system. However, colonization of FAMBR membrane surface by Fe–protein/peptide hydroxocomplexes initiated by Fe-catalyzed microbial extrusions present a huge fouling challenge relative to the AMBR system. Additional evidences from microscopic/spectroscopic analysis of the FAMBR membrane system revealed that despite having a promising outlook, mediation of nano-Fe with AMBR system might result in a major fouling event

* Corresponding authors.
E-mail addresses: okabass@ntu.edu.sg (O.K. Abass), kszhang@iue.ac.cn (K. Zhang).

https://doi.org/10.1016/j.jhazmat.2020.122666
Received 20 February 2020; Received in revised form 30 March 2020; Accepted 4 April 2020
Available online 10 April 2020
0304-3894/

during HFF treatment. Engineered design of nano-Fe to reduced leached nano-Fe ions in pre-treatment step prior to AMBR treatment system may be of potential research consideration.

1. Introduction

The global decline of conventional oil and gas reserves have initiated a hot search for alternative energy sources. According to a recent report, the gap between renewable (13.4 %) and non-renewable (81.6 %) energy sources in the primary energy supply worldwide, remains too wide to be tied up in the coming decades (Melikoglu, 2014). The hydraulic fracturing process, which produces hydrocarbon from shale gas and tight oil rocks serves as an alternative non-renewable energy source and can partly substitute the depleting conventional oil gas resources. Thus, the dependency on conventional oil and gas supplies is reduced at least within the transition period to an economy with higher dependence on renewable energy sources.

After the initiation of the hydraulic fracturing or fracking process, a mixture of the fracturing fluid and formation water also known as connate water will flow back to the surface within days having salinity less than the connate water. This mixture is what is coined "flowback" or "hydraulic fracturing wastewater" in the literature (Kondash et al., 2018). A recent report detailed that water used during hydraulic fracturing process have risen seven-fold in the US during the last six years due to advancement in the technologies used in the fracking processes (Kondash et al., 2018). There are also pressing concerns about the water-intensive nature of the hydraulic fracturing process especially in dry regions as witnessed in Northwestern China (Bergmann et al., 2014; Rahm and Riha, 2014; Jiang, 2009). Moreover, fracturing flowback fluid contains highly varied mixture of toxic elements, naturally occurring radioactive substances, friction reducers, surfactants, gelling agents, corrosion and scale inhibitors, pH and acids regulating agents, salts, and transformation products that could compromise the local ecosystem if mismanaged or spilled into the environment (Ferrer and Thurman, 2015; Gregory et al., 2011; Stringfellow et al., 2014). Though, it has been reported that 50–90 % of these compounds can be degraded biologically via aerobic processes, some toxic organic and inorganic compounds in HFF like PAHs and heavy metals (including Cr, As, Cd, Zn and so on) are not easily removed via direct treatment with biological processes due to their refractory nature (Abass et al., 2017; Sun et al., 2017). Thus, there is need for technologies that can be used to modify the chemical characteristics of HFF streams in order to enhance their treatability in biological systems. Advanced oxidation processes (AOPs) (Abass et al., 2017; Zielinska-Jurek et al., 2017; Tang et al., 2019) and Fe-based technologies (Abass et al., 2016; Sun et al., 2019a; Wang et al., 2020a, b; Zhang et al., 2017) are potential HFF pretreatment candidates, which have shown high degradation capacity for a variety of HFF compounds to intermediate biogenic products such as alcohols, aldehydes, and carboxylic acids (Abass et al., 2017).

Fe-based processes including homo (Fenton) and heterogeneous (Fenton-like) processes play important role in the generation of hydroxyl radicals ($^{\cdot}OH$), ferryl ion species (Abass et al., 2017; Xiong et al., 2018) and other reactive agents such as, sulfate/persulfate-based radicals (Wang et al., 2020a, b), which are key radicals responsible for oxidation of refractory organics, such as found in HFF streams. Although, the oxidation of these organics via homo Fenton processes (i.e. $FeSO_4$ and H_2O_2) was quite effective, the homogenous salt (i.e. $FeSO_4$) are rapidly consumed with attendant low oxidation efficiency (Venny et al., 2012; Lin et al., 2016). Recently, concerted efforts have been dedicated to developing Fe-based nanomaterials (nano-Fe) also called nanoscale zero-valent iron to serve as catalyst and adsorbent for oxidation/reduction/adsorption of toxic organic/inorganic pollutants present in HFF streams (Abass et al., 2017; Sun et al., 2017, 2019a; Wang et al., 2020a, b; Zhang et al., 2017). An additional advantage of nano-Fe is its potential to adsorb or reduce various pollutants, including organic chemicals, heavy metal ions, dyes, nitrate, phosphate, and radionuclides due to their high reactivity and large surface areas (Abass et al., 2017; Zhou et al., 2015). However, bare or surface-exposed forms of nano-Fe are reported to suffer efficiency, surface passivation, stability, and corrosion setbacks when utilized directly in wastewater, or in more severe matrices, like high saline HFF streams (Sun et al., 2017, 2019a; Sun et al., 2016). Current advances towards addressing this challenge involves the deployment of encapsulated forms of nano-Fe to allow diffusion of reactive Fe ions through the capsule, thus reducing the surface passivation rate and enabling the sustainable reuse of the bare nano-Fe (Sun et al., 2017, 2019a; Zhu et al., 2017). While these are plausible improvement in sustaining the reactivity and longevity of nano-Fe materials, the utilization of bare nano-Fe are preferred in some treatment matrix, especially when the goal of the treatment is to realize high dissolution rate of nano-Fe and in conditions where high salinity is not an issue. In addition, ions dissolution and migration rate in entrapped nano-Fe are limited by the porosity of the entrapping layer. Thus, in this work, bare nano-Fe was used as pretreatment option with integrated biological membrane-based process.

Conversely, biological treatment of pollutants, though environmentally friendly, are less effective for efficient degradation of recalcitrant wastewater due to minimal resistance of microorganisms to toxicity (Kundu et al., 2012). In recent times, membrane bioreactors (MBR) are increasingly used as substitutes for conventional biological treatment processes due to several merits as indicated the literature (Abass et al., 2015, 2018; Krzeminski et al., 2017). However, the individual use of each treatment technology for degradation of HFF are confronted with several challenges as highlighted previously. Increasing number of studies have proposed the integration of Fenton process with biological treatment to improve the biodegradability of oilfield wastewater by generation of biodegradable intermediates before the biological treatment step, and vice versa (Venny et al., 2012; Yu et al., 2015; Chen et al., 2017; Punzi et al., 2015; Giannakis et al., 2015; Khoufi et al., 2009; Vilar et al., 2012; Lu et al., 2010). The combination of this technology becomes necessary due to the high residual chemical compounds found in HFF, which causes foaming during aerobic biological treatment process (Abass et al., 2017).

Pollutants associated with HFF include polycyclic aromatic hydrocarbons (PAHs), which are found at elevated levels in most HFF (Gordalla et al., 2013; Butkovskyi et al., 2017). PAHs have been widely investigated because they can potentially transport in different media (especially in water and air) at long distance range and are toxic at elevated levels. Aerobic and anaerobic biodegradation has been employed to degrade PAHs but were found inefficient, only achieving a degradation efficiency about 20 %–50 % (Butkovskyi et al., 2017). Therefore, treatment by biological means only is not feasible for complete mineralization of HFF pollutants. HFF pretreatment by other technologies may provide adequate treatment efficiency, considered at an acceptable operating cost. However, little is known about effect of the HFF pretreatment on overall performance of the treatment system. Recently, Sun et al. (2019b) advanced the importance of combined treatment technology for HFF streams, as no single treatment option is capable of mineralizing the complex HFF streams.

Thus, mediation of nano-Fe with tandem anaerobic-oxic membrane bioreactor (FAMBR) for HFF treatment and resource recovery was evaluated in this study. The nature and chemical compositions of the HFF was comprehensively characterized and their risk potential to drinking water in the area was evaluated based on well-known standards. The direct and indirect influence of the nano-Fe enabled system

on micro-pollutants removal and the nature of sludge flocs in conjunction with flux production rate were respectively investigated at both short and long-term conditions. Similarly, the complex interactions of nano-Fe ions sensitized sludge matrix with parallel AMBR membrane systems were explored.

2. Materials and method

2.1. Experimental set-up and operating conditions

Prior to the integrated operation, dosage optimization test of the nano-Fe (average particle size ≤100 nm, purchased from Aladdin Chemical Co. Ltd, Shanghai) was conducted using continuous stirred tank reactors (Model ZR4-6, Shenzhen, China) operated in batch mode. The optimization test were performed at ambient temperature (22 ± 2 ˚C) in 1000 mL glass beakers and under oxic conditions (at airflow rate of 1.5 L/min) using varying concentrations of nano-Fe (0, 0.03, 0.045, 0.1, 0.5, 1.0, 2.0, and 3.0 g) per liter of HFF and hydrogen peroxide were added in stoichiometric amount following the theoretical amount of hydroxyl radicals generated per mole of nano-Fe. Caution was taken to ensure that the fresh nano-Fe were not exposed to ambient air prior to addition in batch reactors (as the elemental iron nano-powder can be spontaneously oxidized, and easily ignited on contact with air). However, it should be noted that air-stabilized nano-Fe is more suitable for field application. Results obtained from the nano-Fe optimization experiments were reported in Abass et al. (2017) and were scaled-up for the semi-pilot scale hybrid treatment as shown in Fig. S1. The uptake and removal of inorganic metals ions and organic compounds by nano-Fe were investigated.

Two parallel treatment sets with and without pre-treatment with nano-Fe were designed and built at the Urban Pollution Conversion Centre of the Institute of Urban Environment, Xiamen. The first treatment set is a tandem anaerobic-oxic MBR (AMBR) system, while the hybrid treatment set comprise a nano-Fe pretreatment integrated with anaerobic-oxic MBR (FAMBR) system (Fig. 1 and Fig. S1 of Supplementary Information). Detailed description of the set-up can be found in SI. The nominal pore sizes of the MF membrane range from 0.25 – 0.28 μm with an effective area of 0.112 m^2. Prior to operation, all reactors were inoculated with sludge from a nearby wastewater treatment plant and acclimatized. Based on the pre-designed hydraulic condition, the reactors (AMBR and FAMBR) were filled with sludge in equal amounts to ensure similar operating conditions in the parallel sets.

The HFF influent input was conducted using peristaltic pumps (Model YZ1515x, LongerPump), which fed the HFF and nano-Fe pretreated HFF to the AMBR and FAMBR treatment sets, respectively. In the nano-Fe pretreatment system, batch runs were conducted in a 70 L-capacity continuous stirred reactor, which produced 40 L per day of pre-treated HFF. Depending on the final pH of the reaction (which is averagely around 6.0 after the reaction), pH adjustment was conducted using 1.0 M H_2SO_4 and 1.0 M NaOH while being homogenized by a stirrer. The AMBR and FAMBR anaerobic hydrolysis reactors were maintained at 30 ± 1 ˚C by a thermostatic heater. A recirculation ratio of 1.33 was adapted for the return sludge between the sedimentation tanks and the anaerobic reactors. To maintain suspension of mixed liquor in the MBRs, scour the membranes, and keep the dissolve oxygen (DO) level at reasonable range, aeration of the membrane were constantly operated at SAD_m (specific aeration demand) of 1.6. DO concentrations in the anaerobic reactor and MBR were maintained at < 0.1 mg/L and ~ 4.5 mg/L, respectively. Two pressure transducers were electronically wired to a data logger (PicoLog version 5.22.9 by Pico technology), which continuously measures and record the transmembrane pressure (TMP).

The permeate operation was conducted in a filtration/relaxation mode of 10 min on/ 2 min off and at a constant flux (membrane flux, 13.4 LMH) by adjusting the pumps speed to meet the daily flux production. The pump speed adjustment mode was terminated when consistent increase in pump speed failed to yield the required daily flux production. Cleaning operation was not conducted during the whole experiment for peculiar reasons 1) to ascertain the fouling propensities of the as-received membranes under the defined operating conditions, 2) to quantify the overall effect of possibly leached iron nanoparticles on the FAMBR filtration operation and 3) to simulate periods necessary

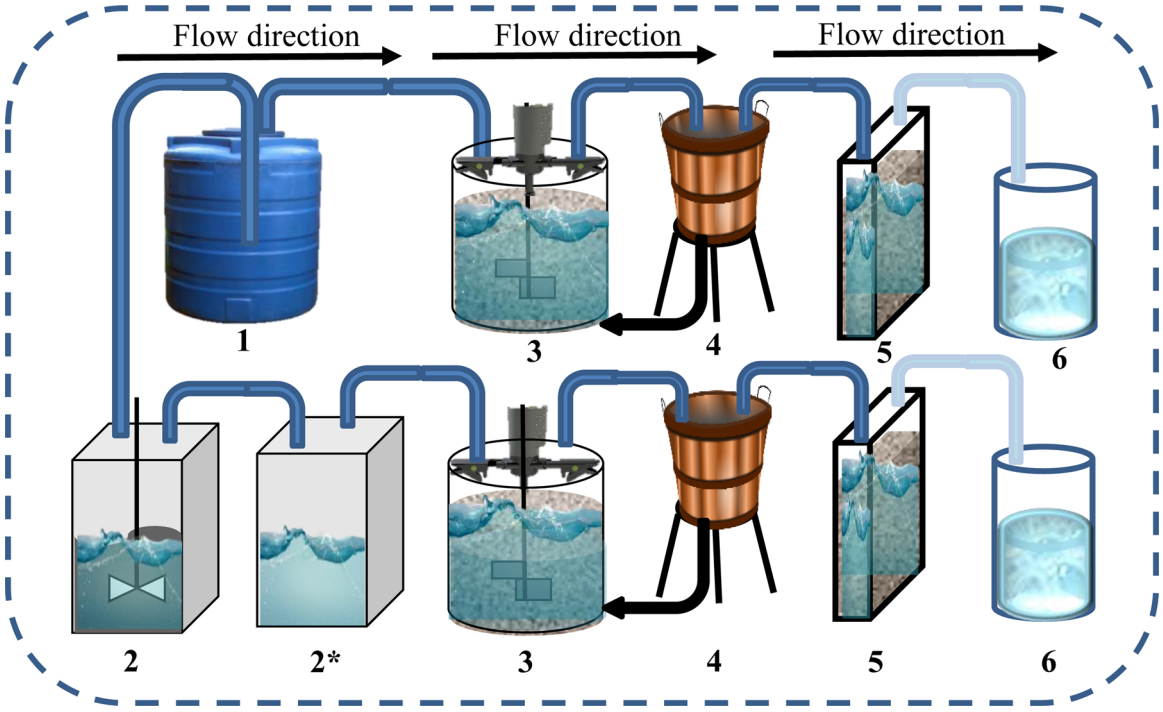

Fig. 1. Schematic of the AMBR and FAMBR systems for the treatment of hydraulic fracturing flowback fluid (1. Influent storage tank, 2. nano-Fe HFF pretreatment reactor, 2*. pH adjustment tank, 3. Hydrolysis anaerobic reactors 4. Sludge settling tanks 5. Membrane bioreactors with submerged flat sheet membranes 6. Effluent storage tank).

for membrane cleaning when put to use in an industrial settings. The MBRs were shut down once the TMP exceeds 25 kPa. Mixed liquor in MBRs of both treatment sets were wasted at least twice a week by retrieving 100 mL of mixed liquor from each MBR for measurements. Total HRTs of the AMBR and FAMBR treatment sets were maintained at 18.6 h–20.7 h and 18.6–36.9 h, respectively. The pH (AMBR = 7.1 ± 0.1, FAMBR = 6.8 ± 0.2) varied slightly during the whole treatment duration for both reactors.

2.2. Fouling analysis and derived parameters

The fouling characteristics of the MBRs were determined using fresh and fouled membrane samples retrieved from the treatment sets. Triplicates samples of the fouled membranes were detached at different points from the membrane holder and their corresponding fouling resistances were tested via a dead-end filtration cell (Amicon Stirred Cell Model 8010) at a pressure of 20 kPa driven by nitrogen gas. In this study, deposition of activated sludge mixed liquor and interrelated components on the membrane surface, which created the fouling layer was considered. According to Darcy's Law, the relationship between TMP in Pa, and permeate flux (J) of the pristine and fouled membranes ($Lm^{-2}\ h^{-1}$ or LMH) can be described by resistance in series model as shown in Eq. (1).

$$J = TMP/\mu(R_m + R_{tf}) \quad (1)$$

where μ is the dynamic viscosity of the permeate in (Pa s), R_m is the resistance of the pristine membrane (m^{-1}), and R_{tf} is the total resistance resulting from different fouling types (m^{-1}). Resistances of the pristine membrane, reversible and irreversible fouling layer were derived as follows. (a) R_m was computed from the clean water permeability of the membrane before the experimental start-up; (b) sum of the resistances of the pristine membrane and fouled layer (reversible or irreversible) were computed from the clean water permeability of the fouled membranes after experiment; (c) sum of the resistances of the pristine membrane and irreversible fouling layer were derived from the clean water permeability of the fouled membrane after membrane cleaning (using 100 mg/L citric acid at pH 3.5, for 24 h and 1000 mg/L sodium hypochlorite at pH 11.3, for 24 h). Accordingly, the reversible and irreversible fouling resistances were computed following Eq. (1). The permeability recovery (P_R) ratio of the membranes were also derived using the average clean water permeability of cleaned or fouled membranes (P_{RC}) and pristine membranes (P_{RP}). The P_R ratio was expressed in percentage as shown in Eq. (2).

$$P_R = {P_{RC}}/{P_{RP}} \times 100\% \quad (2)$$

2.3. Analytical standards and methods

Standard Methods were used for COD, total dissolved solids (TDS) and total and volatile suspended solid (TSS &VSS) (APHA, 2005) measurement. TOC analyzer (TOC-V_{CPH} analyzer, Shimadzu, Japan) was used for TOC and TN analysis. Analysis of the inorganic ions, metals and heavy metals content of the HFF was carried out using an ion chromatograph (Dionex ICS 3000), Perkin Elmer inductively coupled plasma optical emission spectrometer (ICP-OES, Optimal 7000DV), and an inductively coupled plasma mass spectrometer (ICP-MS, Agilent Tech. 7500 Series), respectively. After HFF treatment via the nano-Fe pretreatment reactor, and prior to flow operation into the bioreactors, samples were withdrawn from the supernatant and filtered using a 0.22 μm PTFE membrane for further analysis.

Extraction of PAHs was carried out in an ultrasonic bath (40 kHz, KQ500DE, China) at 500 W, as previously described by Lin et al. (2016). See supporting information for more details. X-ray fluorescence spectroscopy (XRF) was used for the qualitative and quantitative analysis of the recovered metals and inorganic components of the HFF detected on a ZB Axios-mAX spectrometer. Fourier transform infrared (FTIR) measurement was used to investigate the organic and inorganic components of the fresh and fouled membrane using FTIR spectrophotometer (The Frontier FTIR, PerkinElmer, USA). The instrument limit of determination and sample preparation methods are described in Abass et al., 2018. Other method and instrumentation limits used are described in supporting information.

2.4. Characterization of mixed liquor and membrane foulants

50 mL sludge samples were retrieved bi-monthly from the reactors to quantify the mixed liquor suspended solids (MLSS) and the mixed liquor volatile suspended solids (MLVSS) concentrations (an index of microbial growth in the bioreactor systems) via Standard Methods for MLSS and MLVSS analysis (APHA, 2005). The sludge cake on membrane foulant layers were also measured by carefully scraping off the sludge cake on the membrane surface with a non-adhesive collector. In addition, floc sizes distribution of the sludge mixed liquor were determined using a Malvern Mastersizer 3000 instrument (Hydro LV, UK) with a detection range of 10 nm to 3.5 mm. Each sample was quantified in triplicates and their average value is presented. Procedures for samples preparation for SEM and EDX analysis are detailed in SI.

3. Results and discussion

3.1. HFF characterization

Characteristics of major constituents of the HFF are presented in Table 1. The mean TDS concentration of the HFF was 2397.5 mg/L, which is lesser than the typical range for HFF and produced water from most fracking wells (Gregory et al., 2011; Stringfellow et al., 2014; Lester et al., 2015). The HFF characteristically moderate to low salinity

Table 1
Some characteristics of the raw hydraulic fracturing flowback.

Parameter	Analytical Method	Raw HFF
Bulk Parameter		
pH	HACH	7.0–7.2
TOC (mg/L)	SM 5310B	1047.1–1389.9
TN (mg/L)	SM 5310B	42.5–45.6
COD (mg/L)	EPA 5220D	1400.0–2581.0
TDS (mg/L)	SM 2450C	2280.0–2515.0
PAHs (mg/L)	GC-MS	0.14–0.42
TSS (mg/L)	SM 2450D	110.0–11425.0
VSS (mg/L)	SM 2450E	n.d–5140.0
Turbidity (NTU)	HACH 2100N	371.0–1822.0
Inorganic ions		mg/L
SO_4^{2-}	IC	3.30–6.45
F^-	IC	62.4–68.1
Cl^-	IC	2347.5–2410.2
Metals & non metals		mg/L
Mg	ICP-OES	38.2–62.0
Ca	ICP-OES	526.5–946.3
Si	ICP-OES	14.1–17.8
Fe	ICP-MS	0.345–6.83
Zn	ICP-MS	0.0056–0.072
Sr	ICP-MS	2.14–30.83
Al	ICP-MS	0.14–0.36
Cd	ICP-MS	0.00013–0.0073
Ni	ICP-MS	0.013–0.038
Sb	ICP-MS	0.0038–0.0075
Cr	ICP-MS	0.0028–0.0057
As	ICP-MS	0.0025–0.015
Mn	ICP-MS	0.126–0.85
Co	ICP-MS	0.0011–0.0019
Pb	ICP-MS	0.001–0.007
Ba	ICP-MS	0.636–0.686

n.d – not detected.

revealed that it is of non-marine origin (Tang et al., 2017), and contain relatively less concentrations of scale forming ions such as Ca, Mg, Ba, Si, and Sr (Table 1). All samples retrieved from the site possess a near neutral pH 7.1 ± 0.1. Other important quality parameters including TOC (average at 1218.5 mg/L), turbidity (371–1822 NTU), TSS (110–11425 mg/L) and total nitrogen (42.5–45.6 mg/L), were all within typical ranges previously reported for HFF except for the TDS, as the HFF was recovered from a continental shale reservoir (Tang et al., 2014), which is basically different from other source rocks reported in the literature (Lester et al., 2015; Zeng et al., 2020). Comparatively, the mineralogy of Marcellus, Barnett, and Eagle Ford shale plays for instance, contain 71.30 %, 77.55 %, and 66.80 % calcite ($CaCO_3$), respectively while Yanchang shale play contain an average of 3% calcite (Tang et al., 2014; Zeng et al., 2020). Similarly, chloride concentrations in Marcellus and Longmaxi formation in the Weiyuan gas field, Sichuan Basin, China are 300, 000 mg/L and 50,000 mg/L, respectively (Ni et al., 2018; Yu et al., 2016). Moreover, the TDS concentration observed in HFF derived from Yanchang formation and Shengli Oilfield, China were around 2280–9630 mg/L and 6850 mg/L, respectively (Abass et al., 2017; Yang et al., 2014). Thus, these discrepancies in salt concentrations implies that dissolved salts in HFF from different shale plays differs significantly. However, the distinctiveness in the salinity of this study HFF samples may be that the HFF samples were taken few days after fracking operation from a shallow lacustrine fracked well with less interaction with formation connate water, as compared to those taken from wells with high interaction with connate formation brine such as the Longmaxi and Marcellus shale play (Zeng et al., 2020; Ni et al., 2018). It is also important to note that interaction of slick water (i.e. fracking fluid) with connate formation brine and pre-existing dissolved salts in reservoir rocks has been identified as the main reason for the characteristics high salinity of HFF (Zeng et al., 2020), and the longer the interaction, the higher the HFF salinity, which explains why samples taken many days after fracking operation tends to possess higher salinity.

Heavy metals including As, Cr, Pb, Cd, Mn and Co were detected in the HFF, which were also found in the work conducted by Ziemkiewicz and He, 2015. Metals concentrations of Sb, As, Ni and Cd all exceeded the drinking water maximum contaminant level (MCL) (see Table 1), which suggests that these metals were either mobilized during fracking operation or originate from the formation brine (Gordalla et al., 2013; USEPA, 2009). Concentrations of anions in the HFF like fluoride was 16 folds higher than the drinking water MCL (USEPA, 2009) (Table 1).

3.1.1. PAHs in HFF

Several PAHs are regarded as prevalent environmental pollutants, hazardous to ecosystems and a potent human health risk due to their mutagenic and carcinogenic properties (Gordalla et al., 2013). The concentration profiles of selected low and high molecular weight PAHs detected in the raw HFF are presented in Table 2. High molecular weight PAHs including IcdPry, DBahA, and BghiPyr, were not detected in the HFF. In the work reported by He et al., 2017, parent PAHs including IcdPry, DBahA, and BghiPyr were also not detected in all tested HFF and produced water samples from the Duvernay Formation, Alberta, Canada. This suggest that, regardless of the source of the HFF (marine or non-marine), occurrence of these set of PAHs are not common in HFF fluids (He et al., 2017).

Till now, there is no conclusive agreement on the threshold for human exposure and ecological risk assessment for PAHs. In China, the only available primary standard for PAHs is the BaP standard of 0.01 μg/L for drinking water (Feng et al., 2009). However, individual PAHs should have varying health/sanitary standard because their toxicities vary considerably. More than two decades ago, Nisbet and LaGoy (Nisbet and LaGoy, 1992) published toxic equivalency factors (TEFs) for different PAHs by setting the toxicity of BaP to 1. Using the TEFs and the BaP standard (Table S1. Supplementary information), the health standards (HS) of other PAHs for drinking water was formulated using the formula;

$$HS = 0.01/TEFs \quad (3)$$

Similarly, based on the ecological receptors and toxic exposure data from known reference values (Wang et al., 2013), possible risk of exposure to PAHs in China surface waters was computed using the hazard quotient (HQ) as presented in Table S2.

$$HQ = EC_{expo.}/TR_{value} \quad (4)$$

where $EC_{expo.}$ is the assumed exposure environmental concentration of the selected PAHs and TR_{value} is the toxicity reference value (which was set according to WHO standards at 0.014 μg/L for BaP in surface water (Wang et al., 2013)). HQ < 1 indicates low exposure risk from the selected PAHs, while HQ > 1 indicates potential risk of the selected PAHs to human through exposure to the ecosystem.

The exposure pathway of concern are surface water and domestic wells since the HFF in this study is of non-marine origin, and surface water utilization is the most important resource of drinking water in the region and other parts of China. Contamination of water bodies by constituents of the HFF fluids may occur from river, lake and stream

Table 2
Characteristics of selected HFF PAHs (Reference standards/values for evaluation, and required dilution to meet the guidelines for drinking water (D_w), surface water (S_w), and groundwater (G_w) are given in terms of dilution factor (D_f) to the power of 10).

PAHs	Raw HFF, μg/L		Ref. standards/values, μg/L			D_f
	Min.	Max.	D_w	S_w	G_w	Before treatment
Naphthalene	61.70	280.61	10.0[b]	–	1.0[d]	10^{-3}
Acenaphthylene	19.41	60.94	10.0[b]	–	–	10^{-1}
Acenapthene	9.81	12.19	10.0[b]	2.14[c]	–	10^{-1}
Fluorene	44.59	59.67	10.0[b]	2.86[c]	–	10^{-2}
Chrysene	2.74	4.71	0.2[a]	0.50[c]	–	10^{-2}
Benzo(a)pyrene	0.29	0.43	0.01[b]	0.57[c]	0.01[d]	10^{-2}
Benzo(k)fluoranthene	0.54	0.87	0.2[a]	0.36[c]	0.03[d]	10^{-1}
indeno[1,2,3-cd]pyrene	n.d	n.d	0.4[a]	0.36[c]	0.01[d]	n.d
dibenz[a,h]anthracene	n.d	n.d	0.3[a]	0.64[c]	0.01[d]	n.d
benzo[ghi]perylene	n.d	n.d	1.0[b]	0.57[c]	–	n.d

–: data unavailable; n.d: not detected.
[a] US EPA maximum contaminant levels (MCL) in drinking water.
[b] Formulated health standards (HS) of PAHs for drinking water.
[c] HQ calculated from geometric mean concentration of individual PAHs in China's surface water.
[d] Threshold of low concern for local and limited groundwater contaminations.

recharge by contaminated groundwater or may result from superterranean/surface accidents associated with the transport, storage and handling of hazardous compounds used as chemical additives in the fracking fluids. The extent of water bodies' contamination by HFF cannot be predicted in a general way. Therefore, different dilution factors (D_f) of the HFF in the water bodies are considered. The HS standard, the primary drinking water standard formulated by the USEPA (2009), the hazard quotient calculated from geometric mean concentration of individual PAHs in China's surface water (Wang et al., 2013), and the threshold of low concern for local and limited groundwater contaminations (Gordalla et al., 2013) was therefore used to evaluate the concentration profile of PAHs in the HFF compared to reference values for the water bodies as shown in Table 2. The HFF PAHs may originate from the formation water (also known as connate water), or from the fracturing fluid.

Total concentration of selected PAHs in the HFF range from 139.1 μg/L to 419.4 μg/L, with the moderately water soluble PAHs such as, NA, Ace, and Fl dominating the HFF PAHs concentration profile (Table 2). Most of the HFF PAHs would meet discharge requirement for drinking water (D_w), surface water (S_w) and groundwater (G_w) only after a dilution of 1:100 or less (Table 2). However, of special concern is NA, which requires a dilution of 1:1000 in order to meet groundwater threshold values. Based on the HQ index for selected PAHs, the potential toxic risk of exposure for Ace and Fl in the HFF was found to have a HQ > 1 (Table 2), which means accidental release of the untreated HFF (often the case for many hydraulic fracturing sites) into surface waters could introduce potentially high PAHs exposure risk. To avoid such accidents, on-site treatment of HFF with effective and efficient micro-pollutants removal technology is recommended.

3.2. Effect of nano-Fe oxidation/adsorption on PAHs removals

PAHs removal by nano-Fe can proceed via oxidative pathway where in-situ generated H_2O_2 and reactive oxygen species can act as effective oxidants for PAHs degradation or via adsorption pathway, where available active sites around the surface of the nano-Fe particles participate in the sorption process. As earlier reported in Abass et al., 2017, we showed that both oxidation and adsorption pathways are involved in the degradation and removal of HFF organics. However, the prevalence of one pathway over the other largely depend on the reaction conditions (such as pH, oxidation and reduction potential), chemical structure, concentration, composition of pollutants, and characteristics of the nano-Fe catalyst/absorbent (Abass et al., 2017; Man et al., 2018; Shanker et al., 2017). Nano-Fe pretreatment of the HFF PAHs was more effective for the degradation of low molecular weight (LMW) PAHs compared to those with higher molecular weights (HMW) as shown in Table 3. For instance, NA and Acy were efficiently degraded/removed at 71.7 % and 92.0 %, respectively compared to Cry and BaP, which were degraded/removed at 13.1 % and 37.7 %, respectively via the nano-Fe pretreatment system. As noted in a report by Liu et al. (2016), catalytic degradation favors removal of LWM PAHs with higher degradation kinetics compared to HMW PAHs, which removal is mainly via adsorption process. Similar observation was made by Man et al. (2018). Thus, this implies that nano-Fe removal pathway for PAHs in HFF favors catalytic degradation process to adsorption process. HMW PAHs are generally non-soluble in aqueous media and are more easily sorbed onto the surface of adsorbents (Butkovskyi et al., 2017).

From Table 3, COD and TOC removal by nano-Fe were relatively low compared to individual PAHs, which were degraded/adsorbed at higher amounts. As we earlier reported in Abass et al., 2017, nano-Fe removal of TOC and COD are relatively low for real wastewater compared to simulated ones, due to the formation of degradation bye-products, which constitutes as degradable organics in the HFF wastewater matrix and are partially sorbed depending on the number of available surface active sites on the nano-Fe catalyst or adsorbent. After nano-Fe treatment, most of the HFF PAHs required none to 10, or 100 fold dilution factors in other to meet requisite discharge standards (Table 3).

3.3. Overall treatment performance of AMBR and FAMBR system

Both AMBRs achieved above average COD and TOC removal during the approximately 125 days of HFF treatment as shown in Figs. 2 and 3. The COD removal efficiencies were 59.9%–93.1% (ave. removal 71 %) for AMBR and 60.1%–97.5% (ave. removal 73 %) for FAMBR at initial COD values of 812.8 ± 560.5 mg/L and 801.5 ± 564.3 mg/L, respectively. However, contrary to our assumption, the COD and TOC removal performance in the FAMBR system wasn't impressive as compared with the AMBR system (Figs. 2 and 3). Within the first 75 days of operation at moderately low COD and TOC loadings (COD ≈ 100 mg/L to 674 mg/L, TOC ≈ 44 mg/L to 339 mg/L), effluent COD and TOC concentrations in both AMBR and FAMBR reactors almost consistently meets Class 2 category of the China National Integrated Wastewater

Table 3
Treatment performance of the AMBR and FAMBR and removal by nano-Fe in the pre-treatment reactor.

Parameter	Unit	Influent HFF Characteristics		Effluent HFF Characteristics		% removal	D_f	% removal	D_f (AMBR)	% removal	D_f (FAMBR)
		AMBR	FAMBR	AMBR	FAMBR	nano-Fe treatment	After nano-Fe treatment	AMBR	After treatment	FAMBR	After treatment
pH		7.1 ± 0.1	6.8 ± 0.2	7.7 ± 0.4	7.6. ± 0.3	–	–	–	–	–	–
TOC	mg/L	105.6 – 699.5	103.8 – 686.7	8.13 – 234.5	4.6 – 236.8	0.017 – 0.018	–	65.5 - 92.3	$10^{*} - 10^{-1}$	66.2 - 95.6	$10^{*} - 10^{-1}$
COD	mg/L	252.3 – 1373.3	237.2 – 1365.8	18.8 – 556.7	15.5 – 545.0	0.01 – 0.06	–	59.5 – 92.5	$10^{*} - 10^{-1}$	60.1 – 97.5	$10^{*} - 10^{-1}$
Temp.	°C	23.0 ± 2.5	23.0 ± 2.0	25.0 ± 1.5	25.0 ± 1.0	–	–	–	–	–	–
NA	μg/L	93.54	27.37	81.66	17.59	70.7	10^{-2}	12.7	10^{-1}	81.2	10^{-1}
Acy	μg/L	20.31	1.63	16.83	1.15	92.0	10^{*}	17.1	10^{-1}	94.4	10^{*}
Ace	μg/L	4.06	4.27	3.77	2.09	–	10^{-1}	7.4	10^{-1}	48.6	10^{*}
Fl	μg/L	19.89	16.87	22.09	14.55	15.2	10^{-1}	0.0	10^{-1}	26.8	10^{-1}
Cry	μg/L	1.57	1.36	1.34	0.80	13.1	10^{-1}	14.8	10^{-1}	49.2	10^{-1}
BaP	μg/L	0.14	0.09	0.13	0.06	37.7	10^{-1}	9.1	10^{-2}	58.3	10^{-1}
BkF	μg/L	0.29	0.13	0.17	0.13	55.3	10^{-1}	41.3	10^{-1}	54.4	10^{-1}
IcdPry	μg/L	0.00	0.00	0.00	0.00	0.00	0.00	0.00	0.00	0.00	0.00
DBahA	μg/L	0.00	0.00	0.00	0.00	0.00	0.00	0.00	0.00	0.00	0.00
BghiPyr	μg/L	0.00	0.00	0.00	0.00	0.00	0.00	0.00	0.00	0.00	0.00

NA – Naphthalene, Acy – Acenaphthylene, Ace – Acenaphthylene, Fl – Fluorene, Cry – Chrysene, BaP – Benzo(a)pyrene, BkF – Benzo(k)fluoranthene, indeno[1,2,3-cd]pyrene (IcdPry), dibenz[a,h]anthracene (DBahA), and benzo[ghi]perylene (BghiPyr).

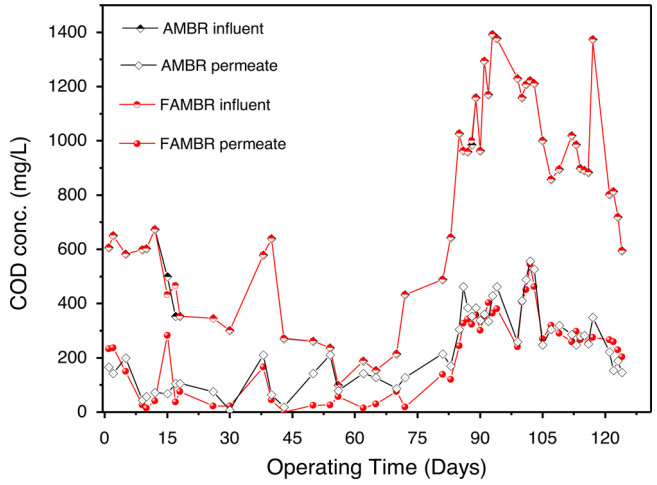

Fig. 2. COD removal characteristics of the AMBR and FAMBR integrated hybrid treatment.

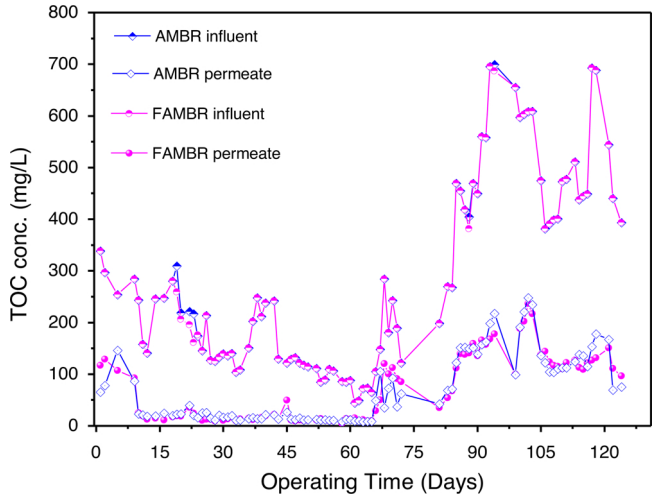

Fig. 3. TOC removal characteristics of the AMBR and FAMBR integrated hybrid treatment.

Discharge Standard (GB 8978 − 1996). However, as the loading rate increased (Figs. 2 and 3), both systems (AMBR and FAMBR), still performed relatively well reaching average COD and TOC removal efficiency of 67.0 % and 71.6 %, respectively for AMBR, and 69.0 % and 72.4 %, respectively for FAMBR. Though, both systems require an average dilution factor of up to 10 fold to meet the aforementioned discharge limit. Moreover, despite the deliberate shock loading (average COD loading ≈ 1038.6 mg/L) during the second stage of the reactors operation (to simulate real life wastewater influent occurrence), the resilience demonstrated by both systems to effectively reduce pollutants load may be primarily due to acclimatization of the microorganisms to the HFF substrates as earlier described by Abass et al., 2018.

To understand the individual reactor process contribution to the reduction of the HFF pollutants load, samples for TOC measurement were retrieved from the anaerobic and oxic MBR reactors of the AMBR and FAMBR systems as shown in Fig. 4. At the onset of the treatment, the anaerobic compartment of the FAMBR achieved a TOC removal efficiency up to 44.7 %, forming the highest percentage of the other two organic pollutants removal pathways (oxic MBR reactor and membrane/sludge cake layer). In contrast with the FAMBR system, the AMBR membrane/sludge cake layer accounted for the highest (41.6 %) organic pollutants removal of the other two pathways. It is clear that the anaerobic and oxic MBR reactors were not actively involved in pollutant degradation during the onset of the treatment. However, from Day 7 onward, the two biological pollutant removal pathways of the AMBR system kicked up, especially the oxic MBR accounting for the highest pollutant removal pathway during the treatment operation (Fig. 4). A similar trend was observed for the FAMBR oxic MBR reactor. This suggests that aerobic microorganisms are more effective for HFF organic degradation compared to anaerobes as also earlier observed by Abass et al., 2018.

As the membrane cake layer builds up (around Day 95–120), the FAMBR membrane/cake layer acquired a higher capacity for organic pollutant removal at an average value of 37.4 %, compared to 26.2 % organic removal capacity of the AMBR membrane/cake layer (Fig. 4). As later explained, accumulation of precipitated Fe ions at the membrane interface may be responsible for the trap or adsorption of the organic pollutants. The concentration of Fe^{n+} (where n = oxidation states of Fe) species released into the influent FAMBR solution during the nano-Fe Fenton-like oxidation process can be seen in our previous report (Abass et al., 2017). These Fe^{n+} ions can be sustained in the solution after the pretreatment step and thus, are capable of generating reactive oxygen species (ROS), which could eventually lead to oxidative stress, causing bacteria death due to cell lysis by ROS (Zhou et al., 2017). This result in the decrease of biomass (see section 3.4), which slightly influence the FABMR organic carbon degradation performance.

The average removal rate of PAHs by AMBR and FAMBR reactors were 9.9 % and 74.0 %, respectively. The removal of PAHs by MBR system has been successfully demonstrated (Wiszniowski et al., 2011), and it was observed that air stripping favored the removal of LMW PAHs while HMW PAHs were removed principally by sorption unto the sludge particle surface followed by air stripping (González et al., 2012). High content of TSS in HFF has been associated with increased

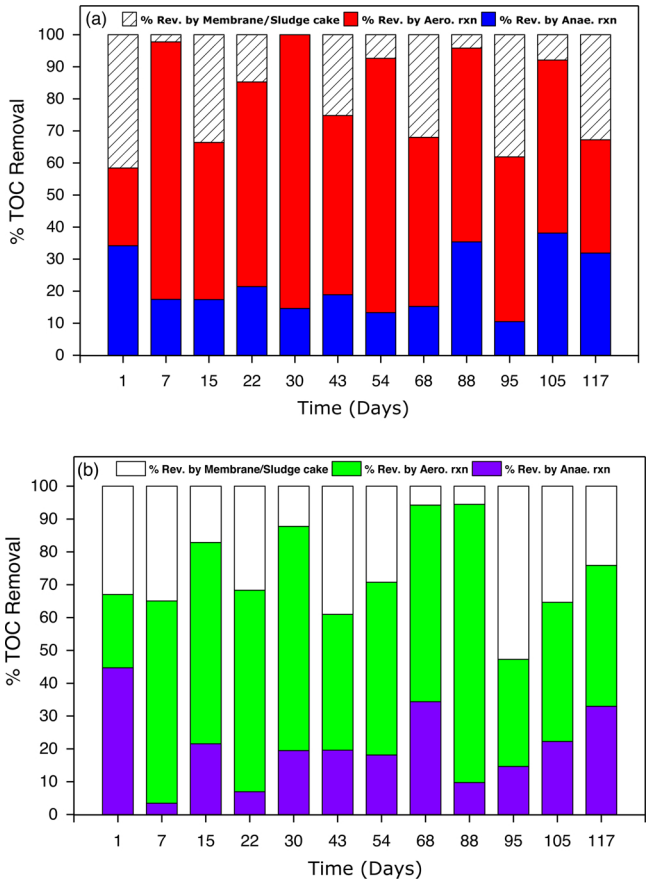

Fig. 4. TOC removal by individual biological treatment unit within the (a) AMBR system and (b) FAMBR system.

concentration of PAHs (compared to HFF with low TSS content), which are capable of inducing lethal and sub-lethal toxicity on life forms in the marine environment (He et al., 2017). As shown in Table 3, compared with the AMBR system, combination of nano-Fe pre-treatment with the AMBR system (FAMBR) enabled higher removal of PAHs by catalytic action of nano-Fe, adsorption on sludge surface, continuous aeration in the MBR and possible biodegradation/biotransformation by micro-organisms as also observed by Haritash and Kaushik, 2009.

3.4. Biomass evolution in the AMBR and FAMBR reactors

The reactors biomass concentration evolution were measured in terms of mixed liquor suspended solids (MLSS) and the volatile components (MLVSS), which are both indicative of the biological activity for the entire duration of the AMBR and FAMBR MBRs runs as shown in Fig. 5. Due to the low total nitrogen concentration in the influent HFF (ca. 14.7 mg/L), recirculation of sludge was not conducted between the anoxic settling tanks and aerobic MBRs tanks. Thus, we describe the biomass concentrations evolution within the MBR systems only.

For the entire operation time, the variation in MLVSS concentrations between the two MBRs was insignificant (Fig. 5). Thus, it is suggested that the possible release and dissolution of Fe ions from the nano-Fe AMBR (FAMBR) system has minimal effect on microbial growth. Similar observation has been made by Xue et al., 2016, where they reported less MLVSS variation between ozonated and non-ozonated oil sands process-affected water treatment by MBR systems. MLVSS/MLSS ratio (an indication of biological sludge fraction viability) was used to evaluate the biomass concentration evolution of the AMBR and FAMBR systems. Earlier, it was reported that the VSS fraction of total suspended solids is between 0.80 – 0.85 (Pollice et al., 2004), however, it was later shown that this ratio can vary even as low as 0.60 – 0.70 under certain circumstances (Menoni and Bertanza, 2016). As presented in Fig. 5, the MLVSS/MLSS ratios in the AMBR and FAMBR MBR systems were between 0.64 – 0.72 and 0.66 – 0.77, respectively, throughout the treatment period, though little variation were observed between the two systems over time.

Generally, low MLVSS/MLSS ratios results in accumulation of inert solids in MBR systems as noted by Judd and Judd (2011). However, in this study both the AMBR and FAMBR MBR systems performed relatively well and are quite consistent with previous studies where oxidation of influent was conducted with oxidative materials (Xue et al., 2016; Feng et al., 2010). Besides, after inoculation of the reactors with the pre-acclimatized sludge, the MLVSS concentration initially decreased before it began to increase on Day 16 for the AMBR system and Day 30 for the FAMBR system. These responses might be related to the influent concentration variation during the treatment operation. The late MLVSS increment response in the FAMBR system might be in addition, due to the Fe ions released into the system as we previously described in Abass et al., 2017. Zhou et al. (2017), observed similar decrease in MLVSS concentration when nano zerovalent iron (nZVI) was loaded unto MBR for membrane fouling control. The decrease in MLVSS was attributed to the increased release of lactate dehydrogenase, which was initiated by bacterial cellular injury and cell death caused by nZVI generated ROS. In this work, a direct response of the MLVSS concentration to variation in influent loading rates was observed. Similarly, the slightly different response of both reactors (AMBR and FAMBR) to the presence of Fe ions is quite pronounced as shown in Fig. 5.

3.5. TMP and membrane fouling development in AMBR and FAMBR reactors

A constant membrane filtration flux design of 13.4 LMH was maintained throughout the whole operation. Therefore, TMP changes were a direct reflection of the membrane fouling development. The TMP and permeability changes over time in the AMBR and FAMBR reactors is presented in Fig. 6a. The initial TMPs in the AMBR and FAMBR were 1.88 kPa and 1.91 kPa, respectively. These were steadily maintained for nearly 21 days after the HFF inoculation before a slight rise in TMP to 2.8 kPa and 3.0 kPa, respectively was observed in both set-ups. As we earlier reported, soluble microbial products and sludge particles in the supernatant could bind to the surface of the membrane, thus generating a resistance, which are capable of blocking the membrane pores leading to increase in TMP (Abass et al., 2015, 2018). The slight increase in TMP resulted in a proportional decrease in membrane permeability (see Fig. 6) and membrane flux from 13.4 to 12.8 LMH for AMBR and 13.4 to 13.1 LMH for FAMBR respectively (Fig. 6). As earlier reported, the particle size of sludge mixed liquor has a significant role in cake layer formation and pore blocking (Zhou et al., 2014). The release of Fe^{n+} in the FAMBR treatment reactor resulted in sludge flocculation as depicted in Table 4. Sludge particle sizes in the mixed liquors of the AMBR and FAMBR were sampled on Day 20, 50, and 75. Samples from the FAMBR produced larger floc sizes (e.g. Day_{50} = 106 ± 4.89 μm) compared to the AMBR system (e.g. Day_{50} = 90.1 ± 1.0 μm) as shown in Table 4. Owing to this, the larger floc sizes gave rise to increase in the sludge filterability regardless of the initial filtration resistance provided by sludge cake layer. This effect was absent in the AMBR system, hence a more drastic flux decline was observed compared to the FAMBR system (Fig. 6b). However, despite the flux decline, the permeability of the AMBR system was still relatively better than the FAMBR system (Fig. 6a). This suggests that the AMBR cake layer was relatively loosely compacted compared to the FAMBR cake layer. The TMPs of both systems remain stable for over two months, which is partially attributed to the anaerobic pre-treatment, flux relaxation steps, air scrubbing effects, long sludge retention time, and the superb anti-fouling resistance of the membrane. However, after 90 days of operation, the FAMBR sustained a gradual but rapid rise of TMP within a week right after increasing the influent volumetric loading twice from 3.11 kg COD/m^3/day to 6.66 kg COD/m^3/day (Fig. 2) with attendant drastic decrease in permeability and flux starting from Day 77 and Day 108, respectively (Fig. 6).

Fouling in the AMBR system was delayed until Day 116, where the TMP began to build up with a corresponding gradual decrease in flux as shown in Fig. 6. As earlier reported, Zhou et al. (2017) and Xue et al. (2016) explained that the use of AOP processes in the pre-treatment of municipal and oil sand process wastewaters favorably decrease membrane fouling in the hybrid AOP-MBR systems utilized, and prolong the membrane cleaning intervals, compared to the control MBR. However, in the FAMBR system described in this study, the increased fouling propensity of the FAMBR system in relation to the control MBR (AMBR)

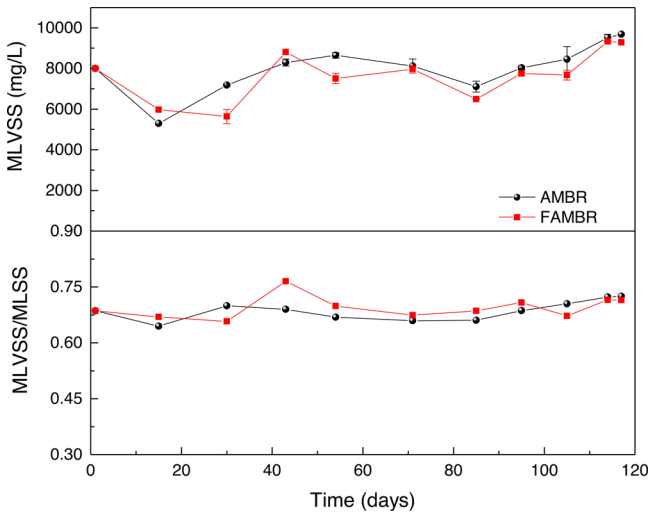

Fig. 5. Bimonthly MLVSS concentration and MLVSS/MLSS ratio over time in the two MBRs (AMBR and FAMBR).

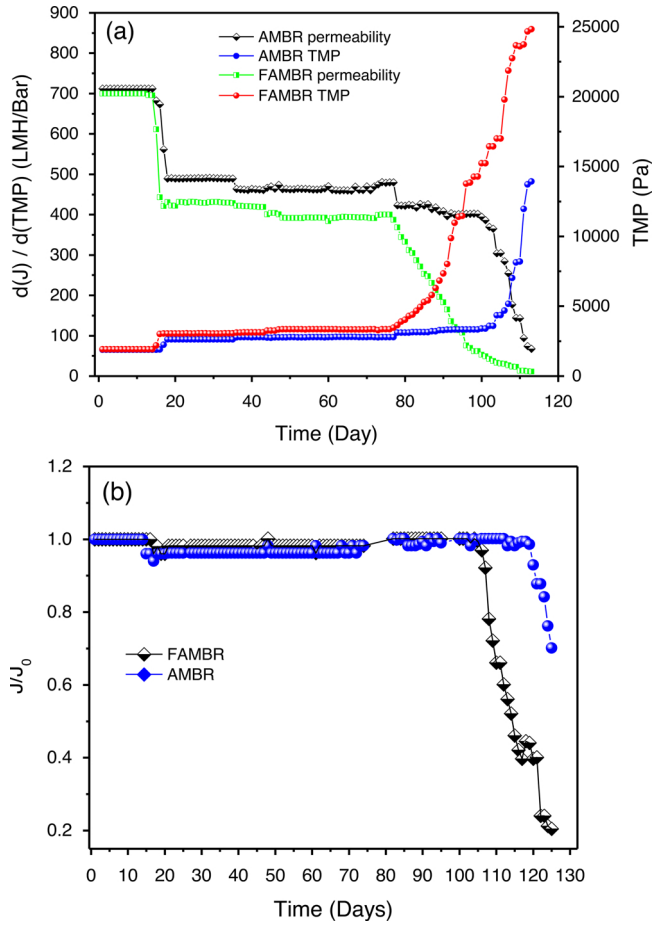

Fig. 6. Variation of (a) permeability and TMP and (b) normalized flux during the parallel operation of the AMBR and FAMBR treatment reactors.

Table 4
Particle size distribution of AMBR and FAMBR mixed liquor sludge.

Sample	Days	D_x (10) μm	D_x (50) μm	D_x (90) μm	Mode μm
AMBR	20	22.1 ± 0.58	68.6 ± 1.4	171.0 ± 7.3	87.9 ± 3.16
FAMBR		27.5 ± 0.71	73.4 ± 1.8	183.0 ± 9.56	96.3 ± 4.56
AMBR	50	21.2 ± 0.29	67.0 ± 0.76	192 ± 2.44	90.1 ± 1.0
FAMBR		23.5 ± 0.51	78.1 ± 1.82	226 ± 12.2	106 ± 4.89
AMBR	75	24.1 ± 0.56	78.6 ± 1.20	199 ± 2.22	97.3 ± 1.33
FAMBR		28.8 ± 1.95	91.0 ± 4.69	216 ± 8.00	109 ± 4.89

D_x represents the diameter where x % of the distribution has a smaller particle size and (100-x) % has a larger particle size.

reveals that different influent type, compositions and processes have significant impact on the fouling propensity of MBRs. In a recent report, hydrolysis of ferric ion in sludge mixed liquor was found to initiate an immediate increase in the extent of fouling (Wang et al., 2014). This effect was apparently due to the production of large numbers of small Fe oxy-hydroxide particles resulting in homogeneous nucleation with the mixed liquor particles, which are capable of blocking membrane pores.

To better understand the fouling mechanism involved in the two MBR systems (AMBR and FAMBR), analysis of the fouling resistance model was conducted. Results showed that both influent HFF constituents and MBR sludge biopolymers (see detailed discussion in section 3.6) influenced the fouling behavior of the two MBR systems. The release of Fe^{n+} in the FAMBR system initiated a synergetic interaction with amino acids and other constituents of the influent HFF within the mixed liquor, which promote the rapid build-up and colonization of the FAMBR membrane surface with a thick particulate cake layer (R_{CL} = 1.42 × 10^{12} m^{-1}) relative to the AMBR (R_{CL} = 0.99 × 10^{12} m^{-1}) (Table 5). A recent work conducted by Wang et al. (2014), concluded that the formation of micro-sized and reactive ferric oxyhydroxide particles are responsible for high membrane filtration resistance observed when iron compound was dosed directly into the reactor anoxic zone prior to flow into MBR. As shown in Fig. 6a and Table 5, the pore blocking effect induced by nano-Fe in the FAMBR system was relatively more pronounced compared to the AMBR system (without nano-Fe).

Further, accumulation of precipitated Fe ions at the FAMBR membrane surface may produce counteractive effect on the microorganism's activities at the membrane-foulant interface. Fe nanoparticles are known to act as direct electron shuttle between interspecies (Suanon et al., 2016). However, at critical conditions (such as in oxic condition and at Fe/microbes non-equilibrium concentrations), ROS could be generated that can cause cell lysis and release of extracellular materials containing hydrophobic components (like proteins), which can be irreversibly bonded to the membrane surface (See Section 3.6). As shown in Table 5, the permeability recovery for both fouled membranes (AMBR and FAMBR) were 19.3 % and 14.2 %, respectively. After rigorous chemical cleaning, the permeability of the AMBR membrane could reach 93.3 %, while the FAMBR's permeability (P_{RC} = 88.4 %) was considerably affected.

3.6. Nano-Fe membrane fouling mechanism

3.6.1. Spectroscopic investigation

Detailed assessment of the fouling mechanism revealed by the functional groups and compositions of the pristine and fouled AMBR and FAMBR membranes was conducted via FTIR analysis, which showed a broad-spectrum absorption from 3334 cm^{-1} to 720 cm^{-1} (Fig. 7). From Fig. 7, the wide and small peaks at 1653 cm^{-1} and 1533 cm^{-1} are respectively due to the stretching vibration of C═O and CN═ of quinone oxime groups (precisely, 4-benzoquinone monoxime) (Ishikawa et al., 1996), indicating that many of the organic compounds in the fouled layer of the AMBR membrane originated from the influent HFF. These peaks were distinctly absent in both the pristine and FAMBR membranes implying that the pretreatment of HFF with nano-Fe initiated the degradation of most micro-organic moieties present in the HFF, which otherwise might have been released back to the environment.

The presence of polysaccharide-like substances at peaks 1089 cm^{-1}, 1014 cm^{-1} and 969 cm^{-1} containing saturated secondary alcohol, cyclic (C—C) alkanes, and OCO—— saturated ether linkage groups were respectively identified on the fouled FAMBR membrane (Luff, 1972). These peaks were not detected on the fouled AMBR membrane, which further confirms the potential activity of Fe ions towards cell lysis and release of biopolymers on the FAMBR membrane surface. Further, as shown in Fig. 7, the fouled FAMBR membrane exhibited a peak at 790 cm^{-1} which corresponds to alpha hydroxyl ferric oxide (α-FeOOH) (Yuan et al., 2013). This peak was completely absent in the AMBR and pristine membrane, respectively. Fe ions are generally known to form coordinate bond with dissociated −COOH groups ($-COO^-$) on the surface of proteins and peptides groups generally produced by

Table 5
Membrane fouling resistances and permeability recovery for AMBR and FAMBR reactors.

Reactor	R_{tf} ($\times 10^{12}$ m^{-1})	R_{CL} ($\times 10^{12}$ m^{-1})	R_{PB} ($\times 10^{12}$ m^{-1})	P_{RF} (%)	P_{RC} (%)
AMBR	1.71	0.99	0.72	19.3	93.3
FAMBR	2.16	1.42	0.74	14.2	88.4

R_{tf} – total fouling resistance; R_{CL} – cake layer resistance; R_{PB} – pore blocking resistance; P_{RF} – permeability recovery for fouled membranes, P_{RC} – permeability recovery for cleaned membranes.

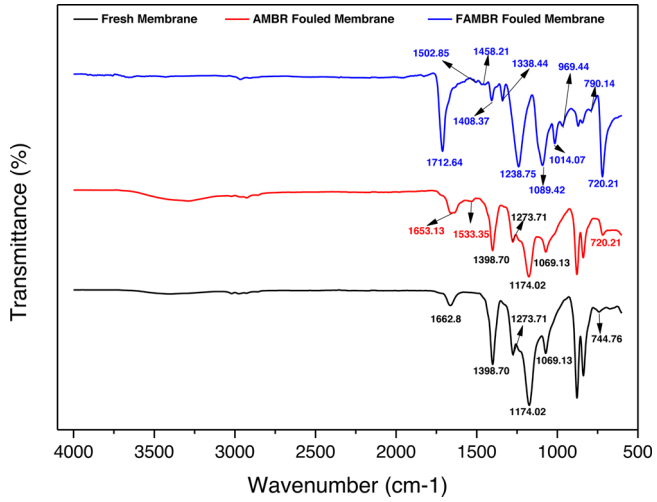

Fig. 7. Fourier transform infrared spectra of the pristine and fouled layer of the AMBR and FAMBR membranes.

microorganisms as extracellular polymeric substances and soluble microbial products (Pivokonsky et al., 2012). As depicted in Fig. 7, these protein/peptide groups are exhibited by peaks 1713 cm^{-1}, 1408.7 cm^{-1} and 1239 cm^{-1} on the fouled FAMBR membrane (note that these peaks were completely absent in the fouled AMBR and pristine membranes) (Luff, 1972).

The coordination of Fe ions with carboxyl groups ($-COO^-$) may initiate the formation of Fe–protein/peptide surface complexes, which are predominantly formed by ionic Fe-hydroxopolymers and Fe-oxide-hydroxides, a cocktail necessary for coagulation (Pivokonsky et al., 2012). The dominance of proteins in form of protonated amino acids, aromatic and aliphatic amines in the fouled FAMBR membrane layer were demonstrated by three unique bands at 1503 cm^{-1}, 1458 cm^{-1} and 1338 cm^{-1}, respectively (Luff, 1972). Protonated amino groups are among the common positively charged proteins moieties. At neutral to basic pH, Fe generally occurs as anionic hydroxocomplexes $(Fe(OH)_4)$–, which are capable of initiating coordinate electrostatic interaction with positively charged proteins moieties (Pivokonsky et al., 2012). Thus, formation of Fe–protein/peptide complexes is significantly increased owing to electrostatic attraction between the proteins and Fe compounds. Consequently, it can be deduced that the rapid fouling of the FAMBR membrane relative to the AMBR membrane may be due to the active interaction of Fe compounds with released protein moieties from microorganisms' by-products or lysed cells.

3.6.2. Microscopic and chemical investigation

The SEM images of the pristine membrane, the fouled AMBR membrane, and the severely fouled FAMBR membrane are illustrated in the Fig. 8. The foulant layer on the surface of the fouled AMBR membrane appears less dense compared to the surface of the FAMBR membrane (Fig. S2), which follows the higher total fouling resistance ($R_{tf} = 2.16 \times 10^{12}$ m^{-1}) observed in the FAMBR system at the end of the treatment operation relative to the AMBR system ($R_{tf} = 1.71 \times 10^{12}$ m^{-1}). Similarly, the partial closing of the membrane pores can be clearly observed from SEM images of the fouled AMBR membrane surface, while a higher amount of blocked pores were observed on the fouled FAMBR membrane surface compared to the pristine membrane (Fig. 8a–c).

Both biofouling and in/organic fouling were found on the fouled AMBR and FAMBR membrane surfaces at the end of the treatment operation. Rod-like and round shaped bacteria were seen on the fouled membranes highlighting the contribution of biofouling in the MBRs fouling process (Fig. 8b and c). Accordingly, the EDX analysis of the pristine membrane revealed that Carbon (98.24 % by weight) dominated the elemental composition (Fig. 8d). Other elements like Na, Si, P, K, Ca, and Fe makes up only 1.76 % by weight of the pristine membrane composition (Fig. 8d). On the other hand, the fouled AMBR and FAMBR membrane surfaces (Fig. 8e and f), revealed the presence of Na, Ca, P and Fe as major inorganic foulants as was previously observed by Wang et al. (2014). However, the release of Fe ions by rapid oxidation of nano-Fe in the FAMBR pre-treatment step varied the distribution of inorganic elements in the membrane foulants compared to AMBR system (Fig. 8e and f). The intensity of metals like Fe and Ca in

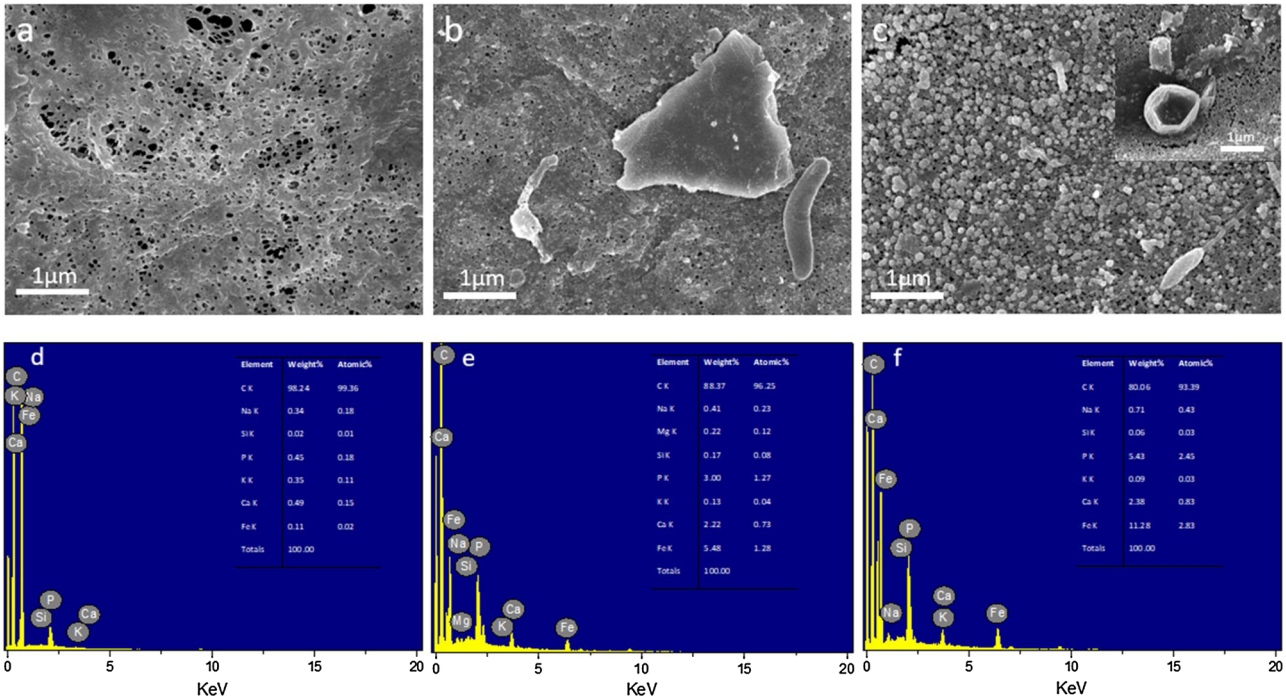

Fig. 8. SEM and EDX images of the (a & d) pristine membrane (b & e) fouled AMBR membrane and (c & f) fouled FAMBR membranes (inset: showing lysed round shaped bacteria with biopolymer release within its vicinity).

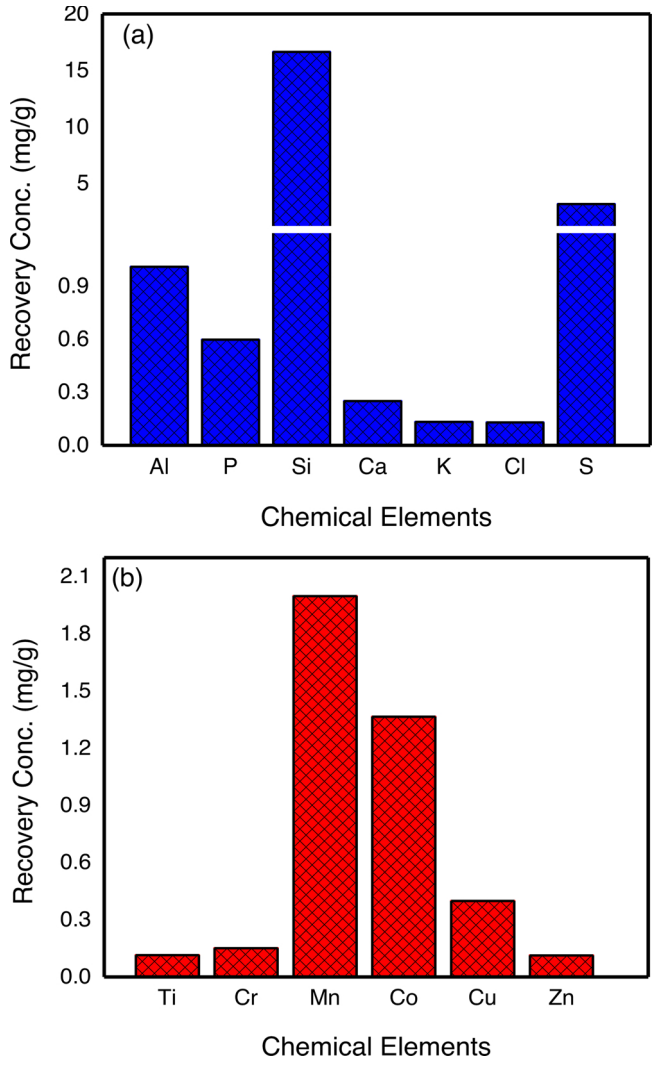

Fig. 9. Average chemical recovery/removal from HFF by nano-Fe for (a) primary metals (b) transition metals.

the foulant layer of the FAMBR membrane (Fe = 11.28 % and Ca = 2.38 % by weight) was considerably higher than those found on the foulant layer of the AMBR membrane (Fe = 5.48 % and Ca = 2.22 % by weight).

The higher abundance of Ca and Fe in the cake layer of the FAMBR membrane compared to AMBR membrane implied the role of those elements to membrane fouling formation. Besides, divalent cations (such as Fe^{2+} and Ca^{2+}) can act as bridges between biopolymers with ionizable groups (such as carboxylic groups) and neighboring organic molecules (such as humic and fulvic acids), thus aiding the electrostatic attraction between them (Volkov et al., 2017). Hence, the increased presence of these metal complexes would aggravate the membrane fouling process through interaction of sludge flocs and biopolymers with the metal ions to achieve charge neutralization as earlier discussed. In addition, metallic carbonates (including $FeCO_3$, $Fe_2(CO_3)_3$ and $CaCO_3$) could be formed owing to the neutral to slight alkaline pH condition in the treatment systems and CO_2 generated via microbial respiration and constant air bubbling in the MBRs. Thus, the higher weight percent of Fe observed on the fouled FAMBR membrane surface is an indication of the presence of ferric fouling relative to the AMBR system.

3.6.3. Resource recovery from HFF by nano-Fe

The recovery of chemicals from the influent HFF by nano-Fe pretreatment was investigated via XRF techniques. The average concentrations of recovered primary chemicals including P, Al, S, Ca, Si, K, Cu, Ti, and Zn were detected at 0.6, 1.0, 3.2, 0.3, 16.6, 0.1, 0.4, 0.1 and 0.1 mg/g spent nano-Fe, respectively (Fig. 9a and b). Other metals adsorbed unto the nano-Fe surface include Cr, Mn, and Co at average concentrations of 0.2, 2.0, and 1.4 mg/g spent nano-Fe, respectively (Fig. 9b). The presence of chlorine (0.13 mg/g spent n-ZVI) in the HFF is indicative of the use of active biocidal agents such as 1-Chloronaphthalene (a colorless oily liquid) to prevent the growth of bacteria in fracked wells. Such chlorinated compounds can react with native materials within the fracked formation to form halocarbons, which can constitutes potential health hazards (Condie, 1985). Therefore, removal of chlorine by nano-Fe in pre-treatment train, represent a potential chlorine detoxification step prior to treatment of HFF in the subsequent biological reactors.

4. Conclusions

A nano-Fe enabled anaerobic-oxic MBR (FAMBR) system has been successfully tested for the degradation and possible reuse of HFF obtained from Yanchang Formation. The following conclusions were made:

1 Compared to the AMBR parallel system, FAMBR system showed superior performance for the degradation of selected micro-contaminants such as PAHs, present in the HFF. Additionally, a resource recovery option for potentially economic metals like aluminum, phosphorus and copper (1.0, 0.6 and 0.4 mg/g spent nano-Fe) availed using the FAMBR system.
2 The nano-Fe mediated treatment phase (FAMBR) and AMBR system displayed slightly similar removal efficiencies for macro/compound organics with maximum COD and TOC removal performance for both system reaching 97.5 % and 94.5 % for FAMBR, and 93.1 % and 92.0 % for AMBR systems, respectively. However, investigation into the systems fouling mechanism revealed that the total fouling resistance (R_{tf} = 2.16 × 10^{12} m^{-1}) of the FAMBR system was relatively higher than the AMBR system (R_{tf} = 1.71 × 10^{12} m^{-1}) as observed at the end of the treatment phase.
3 The fouling event in the FAMBR system were as a result of complex interactions occurring between organic and inorganic substances such as Fe–protein/peptide complexes, precipitated metal ions and Ca carbonate compounds. This poses a major challenge for mediated use of nano-Fe in anaerobic-oxic MBR processes. Future investigations should focus on engineered design of nano-Fe to enable reduction in concentration of leached Fe ions in the pre-treatment step prior to flow into the AMBR system.

Author contributions

Olusegun K. Abass: Designed, conducted all the experiments, analyzed data, prepared the manuscript and provided partial funding for sample analysis.

Kaisong Zhang: Co-designed, coordinated, and provided resources and funding for the project.

Declaration of interest statement

The authors declare no conflicting interest.

Acknowledgements

O.K. Abass acknowledges a Presidential Postdoctoral Fellowship from Nanyang Technological University (NTU), Singapore, via Grant M4082326.030. K.S. Zhang acknowledges the support by funds from the Bureau of Frontier Sciences and Education (QYZDB-SSW-DQC044), and the Bureau of International Cooperation (132C35KYSB20160018),

CAS. Authors are also grateful for funding support provided by Xiamen Municipality Bureau of Science and Technology (3502Z20193073) and Oxiamembrane Co. Ltd., China for supplying the membranes used in the study. We would like to acknowledge the Central Environmental Science and Engineering Laboratory, Nanyang Technological University, Singapore, for use of their testing facility.

Appendix A. Supplementary data

Supplementary material related to this article can be found, in the online version, at doi:https://doi.org/10.1016/j.jhazmat.2020.122666.

References

Abass, O., Wu, X., Guo, Y., Zhang, K., 2015. Membrane bioreactor in China: a critical review. Int. J. Membr. Sci. Technol. 2, 29–47.
Abass, O.K., Ma, T., Kong, S., Wang, Z., Mpinda, M.T., 2016. A novel MD-ZVI integrated approach for high arsenic groundwater decontamination and effluent immobilization. Process Safety and Environmental Protection.
Abass, O.K., Zhuo, M., Zhang, K., 2017. Concomitant degradation of complex organics and metals recovery from fracking wastewater: roles of nano zerovalent iron initiated oxidation and adsorption. Chem. Eng. J. 328, 159–171.
Abass, O.K., Fang, F., Zhuo, M., Zhang, K., 2018. Integrated interrogation of causes of membrane fouling in a pilot-scale anoxic-oxic membrane bioreactor treating oil refinery wastewater. Sci. Total Environ. 642, 77–89.
APHA, 2005. Standard Methods for the Examination of Water and Wastewater, twentieth ed. American Public Health Association, American Water Works Association, Water Environmental Federation, Washington, USA.
Bergmann, A., Weber, F.-A., Meiners, H., Müller, F., 2014. Potential water-related environmental risks of hydraulic fracturing employed in exploration and exploitation of unconventional natural gas reservoirs in Germany. Environ. Sci. Eur. 26, 10.
Butkovskyi, A., Bruning, H., Kools, S.A.E., Rijnaarts, H.H.M., Van Wezel, A.P., 2017. Organic pollutants in shale gas flowback and produced waters: identification, potential ecological impact, and implications for treatment strategies. Environ. Sci. Technol. 51, 4740–4754.
Chen, Y., Lin, J., Chen, Z., 2017. Remediation of water contaminated with diesel oil using a coupled process: Biological degradation followed by heterogeneous Fenton-like oxidation. Chemosphere 183, 286–293.
Condie, L.W., 1985. Target organ toxicology of halocarbons commonly found contaminating drinking water. Science of The Total Environment 47, 433–442.
Feng, C., Luo, Q., Wang, Z., 2009. Concentration levels and potential ecological risks of polycyclic aromatic hydrocarbons in Chinese rivers, water quality. Expo. Health 1, 105–113.
Feng, F., Xu, Z., Li, X., You, W., Zhen, Y., 2010. Advanced treatment of dyeing wastewater towards reuse by the combined Fenton oxidation and membrane bioreactor process. J. Environ. Sci. 22, 1657–1665.
Ferrer, I., Thurman, E.M., 2015. Chemical constituents and analytical approaches for hydraulic fracturing waters. Trends Environ. Anal. Chem. 5, 18–25.
Giannakis, S., Gamarra Vives, F.A., Grandjean, D., Magnet, A., De Alencastro, L.F., Pulgarin, C., 2015. Effect of advanced oxidation processes on the micropollutants and the effluent organic matter contained in municipal wastewater previously treated by three different secondary methods. Water Res. 84, 295–306.
González, D., Ruiz, L.M., Garralón, G., Plaza, F., Arévalo, J., Parada, J., Pérez, J., Moreno, B., Gómez, M.Á., 2012. Wastewater polycyclic aromatic hydrocarbons removal by membrane bioreactor. Desalin. Water Treat. 42, 94–99.
Gordalla, B.C., Ewers, U., Frimmel, F.H., 2013. Hydraulic fracturing: a toxicological threat for groundwater and drinking-water? Environ. Earth Sci. 70, 3875–3893.
Gregory, K.B., Vidic, R.D., Dzombak, D.A., 2011. Water management challenges associated with the production of shale gas by hydraulic fracturing. Elements 7, 181–186.
Haritash, A.K., Kaushik, C.P., 2009. Biodegradation aspects of polycyclic aromatic hydrocarbons (PAHs): a review. J. Hazard. Mater. 169, 1–15.
He, Y., Flynn, S.L., Folkerts, E.J., Zhang, Y., Ruan, D., Alessi, D.S., Martin, J.W., Goss, G.G., 2017. Chemical and toxicological characterizations of hydraulic fracturing flowback and produced water. Water Res. 114, 78–87.
Ishikawa, T., Watanabe, T., Tanigawa, H., Saito, T., Kotake, K.I., Ohashi, Y., Ishii, H., 1996. Nitrosation of phenolic substrates under mildly basic conditions: selective preparation of p-quinone monooximes and their antiviral activities. J. Org. Chem. 61, 2774–2779.
Jiang, Y., 2009. China's water scarcity. J. Environ. Manage. 90, 3185–3196.
Judd, S., Judd, C., 2011. The Mbr Book: Principles and Applications of Membrane Bioreactors for Water and Wastewater Treatment. Elsevier, Oxford.
Khoufi, S., Aloui, F., Sayadi, S., 2009. Pilot scale hybrid process for olive mill wastewater treatment and reuse. Chem. Eng. Process. Process. Intensif. 48, 643–650.
Kondash, A.J., Lauer, N.E., Vengosh, A., 2018. The intensification of the water footprint of hydraulic fracturing. Sci. Adv. 4 eaar5982.
Krzeminski, P., Leverette, L., Malamis, S., Katsou, E., 2017. Membrane bioreactors – a review on recent developments in energy reduction, fouling control, novel configurations, LCA and market prospects. J. Memb. Sci. 527, 207–227.
Kundu, K., Sharma, S., Sreekrishnan, T.R., 2012. Effect of operating temperatures on the microbial community profiles in a high cell density hybrid anaerobic bioreactor. Bioresour. Technol. 118, 502–511.
Lester, Y., Ferrer, I., Thurman, E.M., Sitterley, K.A., Korak, J.A., Aiken, G., Linden, K.G., 2015. Characterization of hydraulic fracturing flowback water in Colorado: implications for water treatment. Sci. Total Environ. 512–513, 637–644.
Lin, M., Ning, X.A., An, T., Zhang, J., Chen, C., Ke, Y., Wang, Y., Zhang, Y., Sun, J., Liu, J., 2016. Degradation of polycyclic aromatic hydrocarbons (PAHs) in textile dyeing sludge with ultrasound and Fenton processes: effect of system parameters and synergistic effect study. J. Hazard. Mater. 307, 7–16.
Liu, B., Chen, B., Zhang, B.Y., Jing, L., Zhang, H., Lee, K., 2016. Photocatalytic degradation of polycyclic aromatic hydrocarbons in offshore produced water: effects of water matrix. J. Environ. Eng. 142, 04016054.
Lu, M., Zhang, Z., Qiao, W., Wei, X., Guan, Y., Ma, Q., Guan, Y., 2010. Remediation of petroleum-contaminated soil after composting by sequential treatment with Fenton-like oxidation and biodegradation. Bioresour. Technol. 101, 2106–2113.
Luff, N.A., 1972. DMS Working Atlas of Infrared Spectroscopy. The University of California, Butterworths.
Man, X., Ning, X.A., Zou, H., Liang, J., Sun, J., Lu, X., Sun, J., 2018. Removal of polycyclic aromatic hydrocarbons (PAHs) from textile dyeing sludge by ultrasound combined zero-valent iron/EDTA/Air system. Chemosphere 191, 839–847.
Melikoglu, M., 2014. Shale gas: analysis of its role in the global energy market. Renew. Sustain. Energy Rev. 37, 460–468.
Menoni, L., Bertanza, G., 2016. Wet oxidation of sewage sludge: a mathematical model for estimating the performance based on the VSS/TSS ratio. Chem. Eng. J. 306, 685–692.
Ni, Y., Zou, C., Cui, H., Li, J., Lauer, N.E., Harkness, J.S., Kondash, A.J., Coyte, R.M., Dwyer, G.S., Liu, D., Dong, D., Liao, F., Vengosh, A., 2018. Origin of flowback and produced waters from Sichuan Basin, China. Environ. Sci. Technol. 52, 14519–14527.
Nisbet, I.C.T., LaGoy, P.K., 1992. Toxic equivalency factors (TEFs) for polycyclic aromatic hydrocarbons (PAHs). Regul. Toxicol. Pharmacol. 16, 290–300.
Pivokonsky, M., Safarikova, J., Bubakova, P., Pivokonska, L., 2012. Coagulation of peptides and proteins produced by Microcystis aeruginosa: interaction mechanisms and the effect of Fe-peptide/protein complexes formation. Water Res. 46, 5583–5590.
Pollice, A., Laera, G., Blonda, M., 2004. Biomass growth and activity in a membrane bioreactor with complete sludge retention. Water Res. 38, 1799–1808.
Punzi, M., Nilsson, F., Anbalagan, A., Svensson, B.M., Jonsson, K., Mattiasson, B., Jonstrup, M., 2015. Combined anaerobic-ozonation process for treatment of textile wastewater: removal of acute toxicity and mutagenicity. J. Hazard. Mater. 292, 52–60.
Rahm, B.G., Riha, S.J., 2014. Evolving shale gas management: water resource risks, impacts, and lessons learned. Environ. Sci. Process. Impacts 16, 1400–1412.
Shanker, U., Jassal, V., Rani, M., 2017. Green synthesis of iron hexacyanoferrate nanoparticles: potential candidate for the degradation of toxic PAHs. J. Environ. Chem. Eng. 5, 4108–4120.
Stringfellow, W.T., Domen, J.K., Camarillo, M.K., Sandelin, W.L., Borglin, S., 2014. Physical, chemical, and biological characteristics of compounds used in hydraulic fracturing. J. Hazard. Mater. 275, 37–54.
Suanon, F., Sun, Q., Mama, D., Li, J., Dimon, B., Yu, C.P., 2016. Effect of nanoscale zero-valent iron and magnetite (Fe3O4) on the fate of metals during anaerobic digestion of sludge. Water Res. 88, 897–903.
Sun, Y., Chen, S.S., Tsang, D.C., Graham, N.J., Ok, Y.S., Feng, Y., Li, X.D., 2016. Zero-valent iron for the abatement of arsenate and selenate from flowback water of hydraulic fracturing. Chemosphere 167, 163–170.
Sun, Y., Lei, C., Khan, E., Chen, S.S., Tsang, D.C.W., Ok, Y.S., Lin, D., Feng, Y., Li, X.D., 2017. Nanoscale zero-valent iron for metal/metalloid removal from model hydraulic fracturing wastewater. Chemosphere 176, 315–323.
Sun, Y., Yu, I.K.M., Tsang, D.C.W., Cao, X., Lin, D., Wang, L., Graham, N.J.D., Alessi, D.S., Komarek, M., Ok, Y.S., Feng, Y., Li, X.D., 2019a. Multifunctional iron-biochar composites for the removal of potentially toxic elements, inherent cations, and hetero-chloride from hydraulic fracturing wastewater. Environ. Int. 124, 521–532.
Sun, Y., Wang, D., Tsang, D.C.W., Wang, L., Ok, Y.S., Feng, Y., 2019b. A critical review of risks, characteristics, and treatment strategies for potentially toxic elements in wastewater from shale gas extraction. Environ. Int. 125, 452–469.
Tang, X., Zhang, J., Wang, X., Yu, B., Ding, W., Xiong, J., Yang, Y., Wang, L., Yang, C., 2014. Shale characteristics in the southeastern Ordos Basin, China: implications for hydrocarbon accumulation conditions and the potential of continental shales. Int. J. Coal Geol. 128–129, 32–46.
Tang, J., Wang, X.C., Hu, Y., Ngo, H.H., Li, Y., Zhang, Y., 2017. Applying fermentation liquid of food waste as carbon source to a pilot-scale anoxic/oxic-membrane bioreactor for enhancing nitrogen removal: microbial communities and membrane fouling behaviour. Bioresour. Technol. 236, 164–173.
Tang, P., Liu, B., Zhang, Y., Chang, H., Zhou, P., Feng, M., Sharma, V.K., 2019. Sustainable reuse of shale gas wastewater by pre-ozonation with ultrafiltration-reverse osmosis. Chem. Eng. J., 123743.
USEPA, U.S.E.P.A., 2009. National Primary Drinking Water Regulations. http://www.epa.gov/safewater/consumer/pdf/mcl.pdf.
Venny, Gan, S., Ng, H.K., 2012. Modified Fenton oxidation of polycyclic aromatic hydrocarbon (PAH)-contaminated soils and the potential of bioremediation as post-treatment. Sci. Total Environ. 419, 240–249.
Vilar, V.J., Moreira, F.C., Ferreira, A.C., Sousa, M.A., Goncalves, C., Alpendurada, M.F., Boaventura, R.A., 2012. Biodegradability enhancement of a pesticide-containing biotreated wastewater using a solar photo-Fenton treatment step followed by a biological oxidation process. Water Res. 46, 4599–4613.
Volkov, I.V., Polyakov, E.V., Denisov, E.I., Ioshin, A.A., 2017. Sorption behavior of strontium ions in humic acid solutions. Radiochemistry 59, 70–78.
Wang, J.Z., Zhu, C.Z., Chen, T.H., 2013. PAHs in the Chinese environment: levels, inventory mass, source and toxic potency assessment. Environ. Sci. Process. Impacts 15, 1104–1112.
Wang, Y., Leslie, G.L., Waite, T.D., 2014. Impact of iron dosing of membrane bioreactors

on membrane fouling. Chem. Eng. J. 252, 239–248.
Wang, D., Sun, Y., Tsang, D.C.W., Khan, E., Cho, D.W., Zhou, Y., Qi, F., Gong, J., Wang, L., 2020a. Synergistic utilization of inherent halides and alcohols in hydraulic fracturing wastewater for radical-based treatment: a case study of di-(2-ethylhexyl) phthalate removal. J. Hazard. Mater. 384, 121321.
Wang, D., Sun, Y., Tsang, D.C.W., Hou, D., Khan, E., Alessi, D.S., Zhao, Y., Gong, J., Wang, L., 2020b. The roles of suspended solids in persulfate/Fe2+ treatment of hydraulic fracturing wastewater: synergistic interplay of inherent wastewater components. Chem. Eng. J. 388, 124243.
Wiszniowski, J., Ziembinska, A., Ciesielski, S., 2011. Removal of petroleum pollutants and monitoring of bacterial community structure in a membrane bioreactor. Chemosphere 83, 49–56.
Xiong, B., Miller, Z., Roman-White, S., Tasker, T., Farina, B., Piechowicz, B., Burgos, W.D., Joshi, P., Zhu, L., Gorski, C.A., Zydney, A.L., Kumar, M., 2018. Chemical degradation of polyacrylamide during hydraulic fracturing. Environ. Sci. Technol. 52, 327–336.
Xue, J., Zhang, Y., Liu, Y., Gamal El-Din, M., 2016. Effects of ozone pretreatment and operating conditions on membrane fouling behaviors of an anoxic-aerobic membrane bioreactor for oil sands process-affected water (OSPW) treatment. Water Res. 105, 444–455.
Yang, J., Hong, L., Liu, Y.-H., Guo, J.-W., Lin, L.-F., 2014. Treatment of oilfield fracturing wastewater by a sequential combination of flocculation, Fenton oxidation and SBR process. Environ. Technol. 35, 2878–2884.
Yu, B., Jin, X., Kuang, Y., Megharaj, M., Naidu, R., Chen, Z., 2015. An integrated bio-degradation and nano-oxidation used for the remediation of naphthalene from aqueous solution. Chemosphere 141, 205–211.
Yu, M., Weinthal, E., Patino-Echeverri, D., Deshusses, M.A., Zou, C., Ni, Y., Vengosh, A., 2016. Water availability for shale gas development in Sichuan Basin, China. Environ. Sci. Technol. 50, 2837–2845.
Yuan, B., Xu, J., Li, X., Fu, M.-L., 2013. Preparation of Si–Al/α-FeOOH catalyst from an iron-containing waste and surface–catalytic oxidation of methylene blue at neutral pH value in the presence of H2O2. Chem. Eng. J. 226, 181–188.
Zeng, L., Reid, N., Lu, Y., Hossain, M.M., Saeedi, A., Xie, Q., 2020. Effect of the fluid–shale interaction on salinity: implications for high-salinity flowback water during hydraulic fracturing in shales. Energy Fuels 34, 3031–3040.
Zhang, H., Xiong, Z., Ji, F., Lai, B., Yang, P., 2017. Pretreatment of shale gas drilling flowback fluid (SGDF) by the microscale Fe(0)/persulfate/O3 process (mFe(0)/PS/O3). Chemosphere 176, 192–201.
Zhou, L., Zhang, Z., Meng, X., Fan, J., Xia, S., 2014. New insight into the effects of Ca(II) on cake layer structure in submerged membrane bioreactors. Biofouling 30, 571–578.
Zhou, H., Shen, Y., Lv, P., Wang, J., Li, P., 2015. Degradation pathway and kinetics of 1-alkyl-3-methylimidazolium bromides oxidation in an ultrasonic nanoscale zero-valent iron/hydrogen peroxide system. J. Hazard. Mater. 284, 241–252.
Zhou, L., Zhuang, W., Wang, X., Yu, K., Yang, S., Xia, S., 2017. Potential effects of loading nano zero valent iron discharged on membrane fouling in an anoxic/oxic membrane bioreactor. Water Res. 111, 140–146.
Zhu, S., Ho, S.-H., Huang, X., Wang, D., Yang, F., Wang, L., Wang, C., Cao, X., Ma, F., 2017. Magnetic nanoscale zerovalent Iron assisted biochar: interfacial chemical behaviors and heavy metals remediation performance. ACS Sustain. Chem. Eng. 5, 9673–9682.
Zielinska-Jurek, A., Bielan, Z., Wysocka, I., Strychalska, J., Janczarek, M., Klimczuk, T., 2017. Magnetic semiconductor photocatalysts for the degradation of recalcitrant chemicals from flow back water. J. Environ. Manage. 195, 157–165.
Ziemkiewicz, P.F., He, Y.T., 2015. Evolution of water chemistry during Marcellus Shale gas development: a case study in West Virginia. Chemosphere 134, 224–231.